Spin waves, phonons, and crystal-field excitations in thulium

Keith A. McEwen
Department of Physics, Birkbeck College, University of London, Malet Street, London WC1E 7HX, United Kingdom

Uschi Steigenberger
Neutron Division, Rutherford Appleton Laboratory, Chilton, Didcot, Oxon OX11 0QX, United Kingdom

Jens Jensen
Physics Laboratory, H.C. Ørsted Institute, DK-2100 Copenhagen, Denmark
(Received 7 March 1990)

The magnetic excitations propagating along the c axis in thulium metal have been studied experimentally by inelastic neutron scattering. At low temperatures, in the seven-layered periodic magnetic structure, the spin-wave energies are centered around 9 meV, with a bandwidth of about 2 meV. A strong coupling to the transverse phonons is revealed through the magnetic scattering cross section. Near T_N clear evidence of crystal-field excitations is found, both in the basal plane and in the c-axis component of the scattering function. A theory based on the random-phase approximation (RPA), which describes the spin waves and the crystal-field excitations in the unusual magnetic structure of Tm, and their coupling to the phonons, is developed. The neutron-scattering results, combined with known magnetization data, have allowed us to derive values for all the relevant coupling parameters. The most important is the two-ion exchange coupling, and the Fourier transform of this interaction along the c direction is presented for all the magnetic heavy rare-earth metals. Except for the linewidth phenomena, which are neglected in the RPA, the calculations account accurately for most experimental details in the antiferromagnetic phase and for the crystal-field excitations close to T_N.

I. INTRODUCTION

With the exception of thulium, the spin-wave excitations in all the magnetic heavy rare-earth metals have been extensively studied, leading to the determination of their fundamental coupling parameters. A practical reason why the spin dynamics of thulium have only recently been thoroughly investigated is the difficulty of growing single crystals of sufficient size for inelastic neutron scattering. This difficulty has now been overcome, and inelastic scattering results for thulium were reported recently by McEwen and Steigenberger,[1] and subsequently by Fernandez-Baca *et al.*[2] It turns out that the interpretation of the data, especially at low temperatures, is not straightforward because of complications introduced by the magnetic structure. We have therefore calculated the scattering function at various wave vectors and compared this directly with the inelastic scattering data.

Like the other heavy rare-earth metals, thulium crystallizes in the hexagonal close-packed structure. The magnetic structure below the Néel temperature $T_N = 57.5$ K has been determined by neutron diffraction,[3,4] and it was found that the c component of the moments is ordered in such a way that it is constant in a particular hexagonal plane but its magnitude changes from one plane to the next. Just below T_N, the oscillatory structure is described in terms of one Fourier component, where the ordering wave vector $\mathbf{Q}$, parallel with the c direction, has a length Q^* of about 0.275 in the reduced unit $2\pi/c$. As the temperature is lowered, higher odd harmonics develop, indicating that the sinusoidal structure begins to "square up." Moreover, the length of $\mathbf{Q}$ changes slightly, until it locks in around 32 K to the value $0.286 \simeq \frac{2}{7}$ which is commensurate with the lattice. Hence the structure repeats itself every seven hexagonal layers. Below this temperature $\mathbf{Q}$ stays constant, locked to the lattice periodicity, but the intensity of the harmonics continues to increase. From the diffraction peak intensities Koehler *et al.*[3] deduced that each c-axis moment reaches its saturation value of $g\mu_B J = 7\mu_B$ in the low temperature limit ($g = \frac{7}{6}$ and $J = 6$ in Tm). The basic periodicity of seven hexagonal layers is then accomplished by four layers with the moments parallel to the c axis followed by three layers with the moments pointing antiparallel to the c axis. This leads to a net ferrimagnetic moment of $1\mu_B$/atom in accord with the magnetization measurements.[5,6]

In this paper we report a comprehensive experimental study of the excitation spectrum of Tm in the c direction as a function of temperature, both in the ordered phase and just above T_N. The size and purity of the crystal used in the present experiments was much improved in comparison with the crystal previously investigated by us. This turned out to be quite crucial, as a number of the features reported earlier[1] were not reproduced in the present measurements. They may therefore be rejected as being due either to impurities (possibly hydrogen) or to imperfections in the lattice. Our present results are consistent with those reported just recently by Fernandez-

Baca *et al.*,[2] but are more comprehensive. In particular we have determined the line shape of the excitations with great accuracy, providing key information for the analysis of the results.

At low temperatures, the spin waves are found to lie in a narrow band between 8–10 meV. When the scattering vector is along the c axis, both the nuclear and the magnetovibrational cross sections of the transverse phonons vanish, because the scattering vector is perpendicular to the polarization of the phonons. Nevertheless, weaker peaks below the spin-wave band were found in c-axis scans, at positions suggesting the magnetovibrational cross section for the transverse phonons to be nonzero. It has been proposed[2] that this scattering may be produced by multiple scattering processes, circumventing the selection rules determined from the direction of the polarization vector and of the magnetic moments. However, we prefer to interpret this scattering in terms of a linear coupling between the spin waves and the transverse phonons, where the mixing of the modes then leads to magnetic scattering from the phononlike components. The introduction of a magnon-phonon coupling in the RPA calculations gives a satisfactory account of this scattering, both as a function of q and of temperature, showing beyond any reasonable doubt that this is the right explanation.

With increasing temperature, the low-energy scattering increases, and by 30 K it is considerably more intense than that expected from the magnon-phonon interaction. The basal-plane components of the scattering function do not change much on passing through the transition temperature, and reasonably well-defined excitations are still apparent around 7–8 meV just above T_N. Combining these results with those obtained when the scattering vector has a component in the basal plane, we find that the cc component of the scattering function involves an excitation around 5 meV in the paramagnetic phase, the intensity of which decreases rapidly below T_N. We have interpreted these additional features in terms of crystal-field excitations (or molecular-field excitations in the ordered phase). Thus thulium becomes the only example among the heavy rare-earth metals in which crystal-field excitations are seen in addition to low-temperature spin waves.

In order to describe the low-temperature spin-wave regime and the appearance of crystal-field excitations at elevated temperatures within the same framework, we have developed an RPA theory based on a numerical diagonalization of the molecular-field (MF) Hamiltonian. One essential complication is that the magnetic unit cell in the antiferromagnetic phase of Tm is seven times as long as the unit cell of the hcp lattice, and there is no transformation, as in the case of a helically ordered structure, which reduces this basis. The Fourier transformation leads therefore to seven coupled equations which can only be solved by numerical methods. Hence the magnetic Brillouin zone contains seven spin-wave branches which scatter neutrons with different weights depending on the scattering vector. The RPA theory is further complicated by the need to include the coupling between the magnetic excitations and the transverse phonons at the same wave vector in the magnetic Brillouin zone. By applying this RPA theory, we have developed a model describing both our inelastic neutron scattering results and the previous studies[4–6] of the magnetic structure. This allows us to present, for the first time, the experimental RKKY-exchange interaction in the c direction for all the magnetic heavy rare-earth metals.

The RPA theory is presented in Sec. II, and the MF-RPA model for Tm is established in Sec. III. The experimental conditions are described in Sec. IV. In Sec. V the experimental results are presented and compared with the calculated results, and our conclusions are given in Sec. VI.

II. THE RPA THEORY

The theory is based on the usual magnetic Hamiltonian for the rare-earth metals:

$$\mathcal{H}=\sum_i \left[\sum_{l=2,4,6} B_l^0 O_l^0(\mathbf{J}_i)+B_6^6 O_6^6(\mathbf{J}_i)-g\mu_B \mathbf{J}_i\cdot\mathbf{H} \right] - \tfrac{1}{2}\sum_{ij}\sum_{\alpha\beta} \mathcal{J}^{\alpha\beta}(ij) J_{i\alpha} J_{j\beta} \, . \tag{1}$$

The large parentheses contain the single-ion contributions, involving the crystal-field terms defined with the Stevens operators O_l^m and the Zeeman term. The coordinate (xyz) axes are chosen to be along an a, b, and c axis, respectively, in the hexagonal lattice. The second sum includes both the isotropic RKKY-exchange interaction and the magnetic dipole-dipole coupling. When the wave vector $\mathbf{q}$ is along the c axis, the Fourier transform of the two-ion coupling $\mathcal{J}^{\alpha\beta}(\mathbf{q})$ is diagonal, and we shall define $\mathcal{J}(\mathbf{q})$ to be the basal-plane component

$$\mathcal{J}(\mathbf{q})=\mathcal{J}^{aa}(\mathbf{q})=\mathcal{J}^{bb}(\mathbf{q}) =\mathcal{J}_0+2\sum_{n=1}\mathcal{J}_n\cos(nqc/2) \, . \tag{2}$$

The above equation also introduces the interplanar coupling coefficients $\mathcal{J}_n$. With this definition the cc component is

$$\mathcal{J}^{cc}(\mathbf{q})=\mathcal{J}(\mathbf{q})+\mathcal{J}_D(\mathbf{q}) \, . \tag{3a}$$

Defining $\mathcal{J}_{dd}=4\pi(g\mu_B)^2N/V$, where N is the number of atoms and V the volume (i.e., $\mathcal{J}_{dd}=0.0305$ meV in Tm) then with $c/a\simeq 0.96\sqrt{8/3}$

$$\mathcal{J}_D(\mathbf{q})=-\mathcal{J}_{dd}[0.919+0.816\cos(qc/2) -0.0006\cos(qc)] \, , \tag{3b}$$

when $\mathbf{q}$ is nonzero, otherwise $\mathcal{J}_D(\mathbf{0})=0$. As realized quite recently, the jump in the long wavelength limit made by the longitudinal component of the dipolar coupling, implies that the magnetic dipole coupling, although weak, has significant effects in the heavy rare-earth metals.[7]

The MF approximation is introduced in Eq. (1) by replacing the two-ion part with

$$-\sum_i\sum_{\alpha\beta}(J_{i\alpha}-\tfrac{1}{2}\langle J_{i\alpha}\rangle)\sum_j \mathcal{J}^{\alpha\beta}(ij)\langle J_{j\beta}\rangle \tag{4}$$

allowing a separate consideration of each ion. In the numerical calculations the magnetic structure is assumed to be commensurate with the lattice, i.e., we assume that the structure repeats itself after seven hexagonal layers. This assumption has been retained at temperatures above 32 K, even though the experimental value of Q^* is then slightly smaller than 2/7.

The first step in the calculation is to assume a distribution of $\langle \mathbf{J}_j \rangle$ of the moments at a given temperature. These values are inserted in the MF Hamiltonian for the ith ion, which is diagonalized. The partition function, the free energy, and $\langle \mathbf{J}_i \rangle$ of this ion may then be calculated. By carrying out this calculation for all the different ions in the seven layers, we may derive a new set of moments. This procedure is repeated until self-consistency is obtained. After having determined the distribution of moments at a certain temperature we may calculate the generalized susceptibilities for each of the different ions. We shall consider the Green's functions, which, with a suitable definition of the temporal Fourier transformation, are

$$g_{AB}(i,\omega)=\lim_{\epsilon\to 0}\left[\sum_{ab}^{E_a\neq E_b}\frac{\langle a|A|b\rangle\langle b|B|a\rangle}{\hbar(\omega+i\epsilon)+E_a-E_b}(n_a-n_b)-\frac{1}{k_BT}\frac{i\epsilon}{\omega+i\epsilon}\left[\sum_{ab}^{E_a=E_b}\langle a|A|b\rangle\langle b|B|a\rangle n_a-\langle A\rangle\langle B\rangle\right]\right], \tag{5}$$

where E_a, $|a\rangle$, and n_a are the ath eigenvalue, eigenstate, and population factor, respectively, of the MF Hamiltonian for the ith ion. When the operators A and B are both set equal to $\mathbf{J}_i$ this equation generates the generalized susceptibility tensor, in units of $(g\mu_B)^2$, but with the opposite sign (see, for instance, Ref. 8). The final two-site Green's functions, written as (3×3) matrices, are then determined by the self-consistent equation

$$\overline{\overline{G}}(ij,\omega)=\overline{\overline{g}}(i,\omega)\delta_{ij}-\sum_{j'}\overline{\overline{g}}(i,\omega)\overline{\overline{\mathcal{J}}}(ij')\overline{\overline{G}}(j',j,\omega)\ . \tag{6}$$

In the uniform case, i.e., the paramagnetic or ferromagnetic phase, the equation may be diagonalized, with respect to the site dependences, by a Fourier transformation. In this formulation the RPA theory provides a description of both the crystal-field excitations occurring in the paramagnetic phase and of the spin waves in the ferromagnetic case. In the latter case, the result coincides in the zero anisotropy limit with that derived in the usual linear spin-wave theory (except that it retains the MF-expectation value of J_z in the result for the spin-wave energies). However, the RPA theory is also valid in the presence of arbitrarily large anisotropy, whereas, in contrast, anisotropy effects may only be incorporated in the linear spin-wave theory if they are relatively weak (see Ref. 8 for a more detailed discussion). In the nonuniform case where the moments are ordered ferromagnetically in layers but where the magnetization changes from layer to layer, the spatial Fourier transformation still leaves as many coupled equations as there are layers in one period. This number p is, however, only finite if the ordering is commensurate with the lattice. In order to write down these equations we define the Fourier transforms

$$\overline{\overline{g}}_s(\omega)=\frac{1}{N}\sum_i\overline{\overline{g}}(i,\omega)e^{-is\mathbf{Q}\cdot\mathbf{R}_i}\ , \tag{7a}$$

$$\overline{\overline{G}}_s(\mathbf{q},\omega)=\frac{1}{N}\sum_{ij}\overline{\overline{G}}(ij,\omega)e^{-i\mathbf{q}\cdot(\mathbf{R}_i-\mathbf{R}_j)}e^{-is\mathbf{Q}\cdot\mathbf{R}_i}\ , \tag{7b}$$

where s is an integer and $\overline{\overline{g}}_{s+p}(\omega)=\overline{\overline{g}}_s(\omega)$. Equation (6) then leads to

$$\overline{\overline{G}}_s(\mathbf{q},\omega)=\overline{\overline{g}}_s(\omega)-\sum_{r=0}^{p-1}\overline{\overline{g}}_{s-r}(\omega)\overline{\overline{\mathcal{J}}}(\mathbf{q}+r\mathbf{Q})\overline{\overline{G}}_r(\mathbf{q},\omega)\ . \tag{8}$$

The method we have used for solving the p matrix equations given by Eq. (8) is to let ϵ in (5) stay nonzero but small, and then to find the solution by a simple iteration [after having isolated $\overline{\overline{G}}_s(\mathbf{q},\omega)$ on the left-hand side of the equation]. If ϵ is not chosen to be too small, the procedure is found to converge rapidly, requiring only 10–20 iterations at each value of $(\mathbf{q},\omega)$. This method was also used for calculating the spin-wave spectrum in the distorted helix and conical phases of Ho.[7,9] The nonzero value of ϵ utilized in these calculations means that the response function is only determined with a finite resolution. Since the experimental results themselves are subject to a finite resolution this is not a serious drawback. Moreover, intrinsic linewidth phenomena, neglected within the RPA, may in most cases justify a nonzero ϵ. After having solved Eq. (8) we may determine the correlation function

$$S(\boldsymbol{\kappa},\omega)=-\sum_{\alpha\beta}(\delta_{\alpha\beta}-\kappa_\alpha\kappa_\beta/\kappa^2)(1-e^{-\hbar\omega/k_BT})^{-1}\frac{1}{\pi}\mathrm{Im}[G_0^{\alpha\beta}(\boldsymbol{\kappa},\omega)]\ . \tag{9}$$

This function multiplied by the form factor squared and the Debye-Waller factor determines the neutron scattering cross section. $\boldsymbol{\kappa}$ is the scattering vector of the neutrons.

As mentioned in the Introduction, the experimental results indicate the presence of a coupling between the magnetic excitations and the transverse phonons in the c direction of Tm. In the long-wavelength limit this coupling arises from the magnetoelastic ε-strain Hamiltonian

$$\mathcal{H}_{me}^{\varepsilon}=\sum_i\{\tfrac{1}{2}c_\varepsilon[\epsilon_{13}^2(i)+\epsilon_{23}^2(i)]-B_\varepsilon[O_2^1(\mathbf{J}_i)\epsilon_{13}(i)+O_2^{-1}(\mathbf{J}_i)\epsilon_{23}(i)]\}\ , \tag{10}$$

where $\epsilon_{\alpha\beta}$ is the Cartesian strain tensor, c_ϵ the elastic constant $(4c_{44}V/N)$ per atom, and $O_2^1=\frac{1}{2}(J_zJ_x+J_xJ_z)$ while $O_2^{-1}=\frac{1}{2}(J_zJ_y+J_yJ_z)$. Considering only long-wavelength phonons propagating along the c axis we find

$$\epsilon_{v3}(i)=\frac{1}{2}(iq)\left[\frac{\hbar}{2NM\omega_v(\mathbf{q})}\right]^{1/2}(\beta_{\mathbf{q},v}+\beta^+_{-\mathbf{q},v})e^{i\mathbf{q}\cdot\mathbf{R}_i}\ , \tag{11}$$

where M is the mass of the ions, $\beta_{\mathbf{q},v}$ the phonon annihilation operator, and $\omega_v(\mathbf{q})$ the corresponding phonon frequency, with $v=1$ or 2 denoting the (x or y) direction of the phonon polarization vector. For simplicity, we assume only one ion per unit cell, corresponding to the double-zone representation in the c direction. The dynamic effects of the magnetoelastic Hamiltonian may be included using essentially the same procedure as in deriving the RPA equation (8). Defining the generalized five-dimensional momentum operator $\mathbf{J}^{(5)}\equiv(J_x,J_y,J_z,O_2^1,O_2^{-1})$ and introducing the corresponding (5×5) matrices for the Green's functions by putting A and B equal to $\mathbf{J}_i^{(5)}$ in Eq. (5), the RPA decoupling leads to an expression identical to Eq. (6). Hence Eqs. (8) and (9) also apply, except that $\overline{\overline{\mathcal{J}}}(\mathbf{q})$ is replaced by the frequency dependent (5×5) matrix $\overline{\overline{\mathcal{J}}}(\mathbf{q},\omega)$. The upper left (3×3) part of $\overline{\overline{\mathcal{J}}}(\mathbf{q},\omega)$ is the original frequency-independent Cartesian matrix, to which we have to add the following two terms in the diagonal:

$$\mathcal{J}_{44}(\mathbf{q},\omega)=\mathcal{J}_{55}(\mathbf{q},\omega)=\lim_{\epsilon\to0^+}\frac{B_\varepsilon^2}{4c_\varepsilon}\frac{\omega_0^2\sin^2(qc/2)}{\omega_1^2(\mathbf{q})-(\omega+i\epsilon)^2}\ . \tag{12}$$

This result is derived with (iq) in Eq. (11) replaced by $(2i/c)\sin(qc/2)$, and it applies not only in the long-wavelength limit but at all wave vectors in the c direction, as long as the ε coupling is dominated by contributions from nearest neighbors. The frequency ω_0 is formally introduced by $c_\varepsilon=M(\omega_0c/2)^2$, but it actually refers to the experimental observation[10] that the transverse phonons in the c direction of Tb are well described by the dispersion relation:

$$\omega_1(\mathbf{q})=\omega_2(\mathbf{q})=\omega_0\sin(qc/4)\ . \tag{13}$$

We expect this to be true also for Tm, except that the maximum frequency ω_0 may be slightly different.

Next-nearest neighbor couplings in the c direction may modify the $\mathbf{q}$ dependence in Eq. (12), but it is also possible that other couplings, not present in the long-wavelength limit described by the magnetoelastic Hamiltonian above, may be of importance when q is not small. This is the case in Tb, where a strong magnon-phonon coupling between acoustic and optical modes has been detected in the c direction.[11] By general symmetry considerations we find that a similar coupling in Tm would *not* invalidate the double-zone representation. The selection rules for this type of coupling are the same as for the ε coupling, and thus it is difficult to distinguish between the two mechanisms. There is, however, one weak point in this argument, namely, that the acoustic-optical coupling in the basal-plane ferromagnet Tb violates the symmetry of the simple ferromagnetic phase. This indicates that in the case of Tb the polarization direction of the conduction electrons responsible for the coupling is noncollinear with the localized moments. We think that this behavior is closely related to the nonzero value of the basal-plane component of the moments in Tb. In Tm the localized moments are parallel to the c axis, which thus remains an axis of threefold symmetry. Hence we do not expect the spins of the conduction electrons in Tm to have any nonzero component in the basal plane, and therefore anticipate no acoustic-optical magnon-phonon coupling in the c direction of Tm.

III. THE MF-RPA MODEL FOR Tm

In order to establish a realistic model for thulium we have used many of the arguments developed earlier by Fynbo.[6] The relevant coupling parameters were introduced in the preceding section. There are four crystal-field parameters and five to six interplanar exchange parameters, which yield a satisfactory description of the two-ion coupling, and finally two magnetoelastic parameters.

First we utilize the measurements[5,6] between room temperature and T_N of the bulk susceptibilities parallel and perpendicular to the c axis to determine $\mathcal{J}(\mathbf{0})$. At high temperatures, the susceptibility anisotropy arises predominantly from B_2^0. Knowing the anisotropy effects, the value of T_N gives $\mathcal{J}(\mathbf{Q})$ (these effects increase T_N by about 60%). The comparison obtained between the susceptibility measurements and the calculated results based on our final model for Tm is shown in Fig. 1. We express the $\chi_{\alpha\beta}$ components in atomic units which are $(g\mu_B)^{-2}V/N$ times the usual bulk susceptibilities. From the neutron diffraction intensities at the fundamental and higher harmonics, Koehler *et al.*[3] derived the corre-

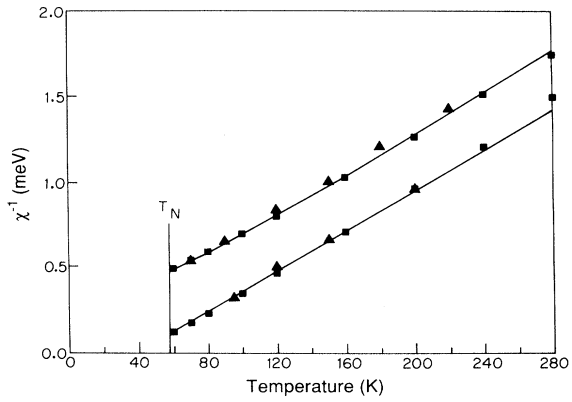

FIG. 1. The reciprocal susceptibilities between room temperature and T_N for Tm. The upper curve is the calculated basal-plane component, and the lower is the cc component. The experimental results are from Ref. 5 (triangles) and Ref. 6 (squares). The unit used is explained in the text.

sponding harmonics of the angular momenta, which are shown in Fig. 2. Although the values of these harmonics are nearly fixed in the zero temperature limit, in terms of the saturation values of the four up–three down structure, the temperature dependence of these quantities is sensitive to the model used. Assuming the crystal-field parameters to be known, these curves establish at least one exchange parameter, which may be considered to be the overall width of $\mathcal{J}(\mathbf{q})$. Given that the maximum of $\mathcal{J}(\mathbf{q})$ has to lie at $\mathbf{q}=\mathbf{Q}$ to a good approximation, we have four to five constraints on the exchange coupling, leaving only about one degree of freedom. Furthermore, there are some additional stability criteria to be fulfilled. The most restrictive requires that $\mathcal{J}_3+\mathcal{J}_4$ is smaller than about -0.025 meV, to prevent the five up–two down structure from occurring when a field is applied in the c direction. Hence the exchange coupling is nearly determined by the magnetization data alone, and the final interplanar coupling coefficients are given in Table I.

The exchange parameters in Table I predict the critical field in the c direction, at which Tm becomes ferromagnetic, to be 4.2 T in the low-temperature limit. However, the first-order transition is actually observed[5,6] at the substantially lower field of 2.8 T. Magnetoelastic effects, not included in the model, may possibly lower the calculated critical field, but only by 0.1–0.2 T. The parameter determining the critical field is the difference between the exchange energy in the two phases, which scales roughly with $\mathcal{J}(\mathbf{Q})-\mathcal{J}(\mathbf{0})$. In the present model, these exchange parameters were derived from the behavior of the system close to T_N. However, in modulated magnetic structures the RKKY coupling may depend on the magnetization. Such a sensitivity is reflected, for instance, in the changes of the ordering wave vector, and other modifications,[7,9] which have been found in Ho. There are two possible mechanisms for explaining the present discrepancy in Tm. The value of the exchange energy difference may gradually decrease with the magnetization when the metal is cooled down, or alternatively, it may change abruptly at the phase transition at the critical field. We have neglected the possibility that the exchange coupling might depend on temperature. If the second possibility dominates, the following analysis is not influenced by the change, as we consider only the antiferromagnetic phase.

In a comprehensive study of the crystal fields of the rare-earth ions in nonmagnetic metallic surroundings, Touborg[12] found that these systems obey the point-charge relation, $B_6^6=-(77/8)B_6^0$, to a very good approximation. The same is true in pure Ho,[7] indicating that it is justified to use this relation for Tm. Two crystal-field parameters then remain undetermined. At low temperatures where the moments are close to their saturation value, the MF ground state and the first dipolar excited

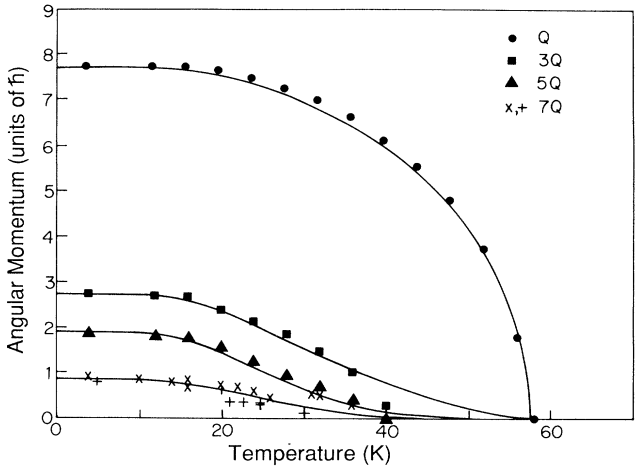

FIG. 2. The different harmonics of $\langle J_{ic}\rangle$ in Tm as function of temperature. The experimental results are taken from Ref. 3. Additional results for the seventh harmonic, the ferromagnetic moment, are from Refs. 4 and 6. The solid lines are our calculated results.

state are almost exactly pure $|\pm 6\rangle$ and $|\pm 5\rangle$ states, respectively (+ or − depending on the site considered), and the crystal-field contribution to the energy difference between these two states is

$$\Delta_{\mathrm{CF}}=-6J_1B_2^0-80J_3B_4^0-336J_5B_6^0\ , \tag{14}$$

where $J_n=(J-\frac{1}{2})(J-1)\cdots(J-n/2)$. This splitting determines the lower bound of the spin-wave energies, which is found to lie near 8.5 meV from the analysis of the inelastic data. The same quantity can be estimated from the basal-plane component of the susceptibility in the low-temperature limit, and χ_{bb} at 4.2 K is calculated to be 0.69 meV^{-1} in atomic units, corresponding to $\langle J_b\rangle\simeq 0.078J$ at a field of 10 T. The experimental values determined in Refs. 5 and 6 are 0.83 meV^{-1} and 1.06 meV^{-1}, respectively. These larger values probably reflect the difficulty of keeping the sample in place when trying to magnetize it along a magnetically very hard axis. B_4^0 in the dilute Tm systems[12] is small and yields a contribution of only -0.6 meV to Δ_{CF}. It might have been acceptable to use this value of B_4^0 for determining the last free parameter in the crystal-field Hamiltonian, as the other crystal-field parameters are close to those derived in the dilute cases. However, the comparison with the experimental low-energy variation of $S(\kappa,\omega)$ at temperatures above 30 K is improved significantly by taking $B_4^0=0$ instead. Our final crystal-field parameters for Tm

TABLE I. The interplanar exchange coupling coefficients in Tm, defined by Eq. (2) and given in units meV.

$\mathcal{J}_0$	$\mathcal{J}_1$	$\mathcal{J}_2$	$\mathcal{J}_3$	$\mathcal{J}_4$	$\mathcal{J}_5$
0.098	0.057	−0.022	−0.025	−0.010	−0.002

TABLE II. The crystal-field parameters for Tm. The first row gives the values derived in the present analysis and the second row those found for Tm diluted in Y, Lu, and Sc (Table IV in Ref. 12). All the parameters are in units of meV.

	B_2^0	B_4^0	B_6^0	B_6^6
Tm metal	-0.096	0.0	-0.92×10^{-5}	8.86×10^{-5}
Dilute Tm	-0.086	0.6×10^{-4}	-0.84×10^{-5}	8.09×10^{-5}

are given in Table II together with the values derived for the dilute systems. Figure 3 shows the energies of the excited crystal field levels as a function of the field $g\mu_B H$.

To our knowledge neither the elastic constants nor the magnetoelastic strains have yet been measured in Tm. Consequently we have used appropriate values determined for the other rare-earth metals. The dispersion relation of the transverse phonons propagating in the c direction of Tm is assumed to be given by Eq. (13). This relates the maximum frequency ω_0 with the elastic constant c_{44} through $c_\varepsilon = M(\omega_0 c/2)^2$. c_{44} has been measured in the other heavy rare-earths, see, for instance, Ref. 13. From the systematic variation of c_{44} through the series, we estimate that its nonmagnetic value in Tm at low temperatures should be $(2.9\pm0.3)\times10^{10}$ J/m^3 corresponding to $c_\varepsilon = 21.8$ eV and $\hbar\omega_0 = (8.35\pm0.4)$ meV. This estimate is consistent with the result $\hbar\omega_0 = 8.5$ meV obtained from calculations[14] of the lattice dynamics in Tm.

The value of the magnetostriction parameter $H_\varepsilon = 2\lambda^\varepsilon$ is 0.02 for Tb in the low-temperature limit.[11] If we assume that this parameter scales with the quadrupolar Stevens factor α, it should be the same in Tm but with opposite sign. In the analysis of the inelastic scattering intensities, discussed in the next section, the best fit is obtained with the estimate $\hbar\omega_0 = 8.35$ meV, and $B_\epsilon^2/4c_\epsilon = 0.0035$ meV for the coupling parameter in Eq. (12). This corresponds to $B_\epsilon = \pm 17.5$ meV and, choosing the minus sign, $H_\epsilon = 2J(J-\frac{1}{2})B_\epsilon/c_\epsilon = -0.053$, which is not so far from the order-of-magnitude estimate derived from the coupling in Tb.

Figure 4 shows the calculated c-axis dispersion relations of the spin waves and transverse phonons in a model corresponding to *ferromagnetic* Tm. However, in order to illustrate the corresponding situation in the antiferromagnetic phase, the dispersion relations have been folded into the magnetic Brillouin zone of this phase,

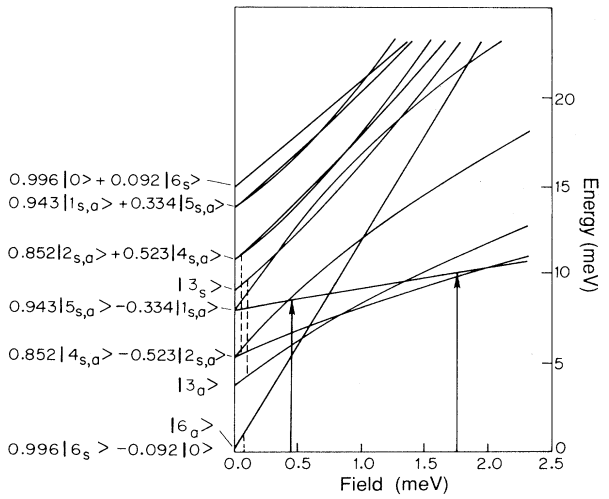

FIG. 3. The crystal-field levels in Tm calculated from the parameters in Table II as a function of the field $g\mu_B H$ (1 meV corresponds to 14.8 T). The state vectors to the left of the vertical axis are the zero field states of the corresponding levels ($|6_{s(a)}\rangle$ denotes the (anti)-symmetrical combination of $|+6\rangle$ and $|-6\rangle$). The vertical lines are referred to in the text.

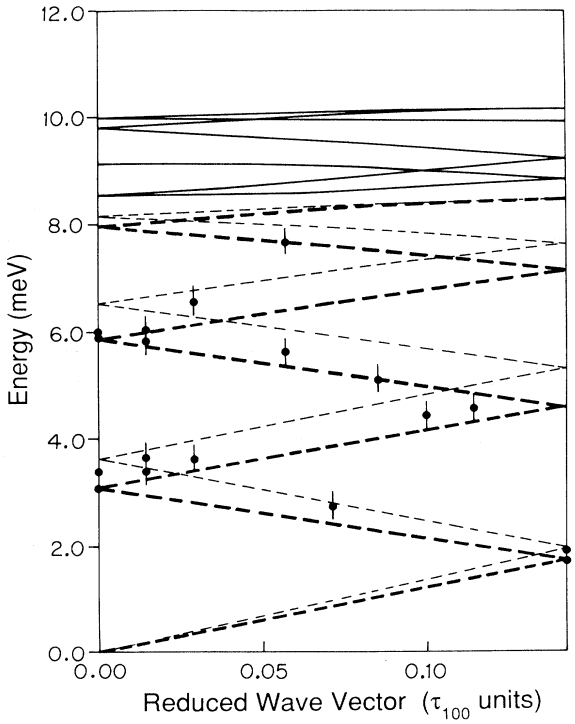

FIG. 4. The dispersion relations along the c direction, at zero temperature, of the spin wave (solid lines) and the transverse phonons (heavy dashed lines) in "ferromagnetic" Tm folded into the magnetic Brillouin zone of the antiferromagnetic phase. The energies of the phonons coupled to the spin waves have been adjusted so as to agree with the results calculated in the antiferromagnetic phase. The thin dashed lines show the dispersion relation assumed for the phonons in the nonmagnetic case. The circles are the experimental results of Fernandez-Baca *et al.* (Ref. 2) for the phonon energies.

which is one-seventh of the lattice zone (the double-zone representation is assumed to be valid). The MF-exchange field was adjusted so that the spin-wave bands lie within the same energy boundaries as in the antiferromagnetic case. Furthermore, the magnetoelastic coupling was reduced slightly in order to obtain the same energies for the phononlike modes as those calculated in the antiferromagnetic phase in the low-temperature limit (except that the possible small energy gaps on the Brillouin-zone boundary do not appear in this ferromagnetic case). The reason for doing this is to show a comparison of the calculated dispersion relation for the phononlike mode with the experimental results reported by Fernandez-Baca *et al.*[2] They made a number of inelastic scattering scans with a component of the scattering vector in the basal plane. In these scans both the magnetovibrational and the nuclear cross sections for the transverse phonons are nonzero, leading to larger intensities from these modes, and thus to a better determination of their energies, than obtained in c-axis scans. As may be seen in Fig. 4 the comparison is satisfactory. If the estimate of the nonmagnetic phonon dispersion relation given above is valid, the phonon energies are clearly reduced from their unperturbed values. These changes amount to nearly 15% at energies between 4–6 meV, and from the slope in the long wavelength limit the resulting magnetic value of the elastic constant is estimated to be 20% smaller than the nonmagnetic one, i.e., $c_{44}^{*}=(2.3\pm0.3)\times10^{10}$ J/m^3 in the low-temperature limit.

IV. EXPERIMENTAL DETAILS

A single crystal of thulium of approximate volume 1 cm^3 was prepared for us at the Ames Laboratory. The mosaic spread of the sample was 30′ . The crystal has a somewhat irregular shape, but faces perpendicular to the principal symmetry directions were cut in order to make the assessment of the absorption correction easier. The experiments reported here were carried out using the thermal neutron triple-axis spectrometer IN8 at the Institut Laue Langevin, Grenoble. Most of the experiments were made using neutrons from a pyrolitic graphite (PG) monochromator, constant-**q** scans were made with the scattered neutron energy fixed at $E_f=14.67$ meV. A PG filter was placed in the scattered beam; appropriate correction was made for the higher order contributions affecting the monitor.

A 40′ collimator was placed in front of the sample and 60′ collimators were mounted before and after the PG analyzer crystal. In this spectrometer configuration the instrumental resolution width (full width at half maximum–FWHM) was 1.0 meV for zero energy transfer and 1.2 meV at 10 meV energy transfer.

The neutron absorption cross section for thulium varies smoothly with neutron energy in the region of interest to us. It is 177 barns at $E_i=14.67$ meV and 140 barns at $E_i=22.67$ meV, corresponding to 8 meV energy transfer. The characteristic distance for a $1/e$ attenuation of the neutron beam is thus 1.7 and 2.2 mm, respectively. Hence absorption corrections need to be considered in making a quantitative comparison of the scattering function at different **q** values.

The measurements were performed with the sample in a standard ILL cryostat, at temperatures between 2 and 60 K. Most of the scans were made with the scattering vector parallel to the c axis.

V. THE MAGNETIC SCATTERING FUNCTION OF Tm

As indicated by Fig. 4 we expect seven different spin-wave branches at each **q** vector. However, the average splitting between these branches is only about 0.3 meV, and it is not possible to resolve them experimentally. The diagonal terms in the coupled equations in Eq. (8) have poles at the same energies as the ferromagnetic spin waves, corresponding to the dispersion relation shown in Fig. 4 if it had not been folded into the magnetic Brillouin zone. Because of the usual dominance of the diagonal terms, the spin-wave structure factor varies such that the lower part of the spectrum dominates for small values of q, in the double Brillouin zone of the reciprocal lattice, whereas the upper part is more important for q^* close to 1 (q^* is q measured in units of $2\pi/c$). The largest off-diagonal terms in (8) are those with $r=s\pm1$. This means that the diagonal excitation at a certain **q** in the Brillouin zone of the lattice is most strongly hybridized with the diagonal ones at $\mathbf{q}\pm\mathbf{Q}$. Similarly it is clear that the magnetic excitation at wave vector **q** is most strongly coupled to the transverse phonons at $\mathbf{q}\pm\mathbf{Q}$. Many features in the experimental results can be understood within this relatively simple framework.

A. Results at low temperatures

Figure 5 shows the inelastic scattering at the three wave vectors (0,0,2), (0,0,2.5), and (0,0,3) in the spin-wave regime between 2–40 K. If we focus first on the results at the lowest temperature, then it is seen that the main peak is centered around 8.5 meV at (0,0,2), and its energy increases slightly with q^* to about 10 meV at (0,0,3). Whereas the peaks at (0,0,2) and (0,0,3) are not significantly broader than the instrumental resolution, the one at (0,0,2.5) has a width of about twice the resolution. In addition to the main peak in each scan, there are some weaker ones at lower energies, for which the intensity and the position change rapidly with wave vector. This is illustrated in more detail by the results at intermediate values of the wave vectors at 2 K, which are shown in Fig. 6. As discussed earlier, we interpret this scattering as originating from a coupling between the magnetic excitations and the transverse phonons. The longitudinal phonons may only couple with the longitudinal magnetic fluctuations, which do not influence the c-axis scans. Since also their energies are higher (about 7 meV already at $q^*=0.3$), the longitudinal phonons should not make any contribution.

The solid lines on the figures show the RPA results derived in Sec. II using the parameters given in Sec. III. In all the calculations we have used $\hbar\epsilon=0.3$ meV [in both Eqs. (5) and (12)]. We have also taken advantage of the fact that the coupled equations can be separated into one set of scalar equations yielding the cc component with the

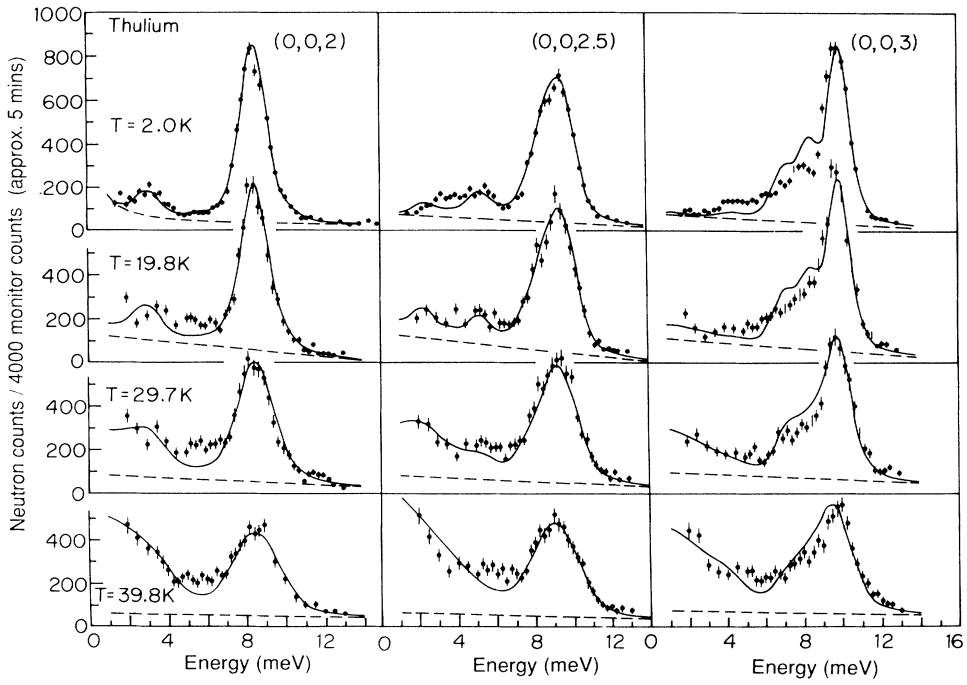

FIG. 5. The inelastic neutron scattering results for Tm between 2 and 40 K at the three wave vectors indicated on the figure. The solid lines represent the calculated results.

remaining set of (4×4)-matrix equations for the other components. The results obtained were then convoluted with a normalized Gaussian, the width of which was adjusted to give the best agreement with the experimental results. In the fit to the data at 2 K, the width was found to be constant between (0,0,2.5) and (0,0,3) but to increase somewhat at the smaller q^* values. Besides this fitting parameter we have, in principle, one overall scale factor accounting for the absolute value of the total scattering intensity, which should change with **q** proportional to the square of the magnetic form factor, not included in $S(\kappa,\omega)$ given by Eq. (9). In practice it turned out that the intensity factor, determined separately at each q^*, increases by about 20% from the (0,0,2) to the (0,0,3) scan, whereas the variation of the form factor[15] suggests just the opposite change. However, this is entirely consistent with the **q** dependence of the neutron absorption. As discussed earlier, all the crystal dimensions are larger than 5 mm, hence the absorption of both the incident and scattered beams is significant. Under these conditions, the absorption will change inversely with κ (or sin θ) at constant energy transfer. The absorption cross sections given in Sec. IV lead to an increase of the intensity factor at (0,0,3) compared to its value at (0,0,2) which is estimated to be about 50%, in good agreement with the observations. The absorption also implies that the intensity factor may depend on the energy transfer in the constant **q** scans. In the scans analyzed here the variations due to the change of the scattering angle and the energy dependence of the absorption cross section very nearly compensate each other, so that the intensity factor is estimated to decrease by only 4–5 %, when the energy transfer is changed from zero to 8 meV. This small correction has been neglected. The final ingredient in the comparison is the background. As may be seen from the figures, the background chosen in the different cases, given by the dashed lines, is well determined in the high-energy limit but some arbitrariness appears at low energies.

The comparisons between the experimental and theoretical results at 2 K, in Figs. 5 and 6, show that the calculations account in considerable detail for the line shape of the spin-wave peaks between 8–10 meV. This indicates that the model presented in Sec. III not only predicts the spin-wave energies correctly, but also puts the right weight on the different branches in the scattering function. The average position of the peaks has enabled us to make an accurate determination of the crystal-field parameter Δ_{CF} given by Eq. (14). The variation of the spin-wave energies and the line shape is determined, to a first approximation, by $\mathcal{J}(\mathbf{q})$. As described in Sec. III the exchange coupling is established almost solely by the magnetization data, and only small adjustments were necessary to fit the present data. The only significant discrepancy was found at (0,0,3) where the lower of the two peaks produced by the spin waves (at 8.5 and 10 meV, the peak at 7 meV is due to the phonons) is calculated to have too high an intensity at the expense of the upper one. In spite of many attempts, we were not able to remove this discrepancy without drastically worsening the close agreement obtained at the other **q** vec-

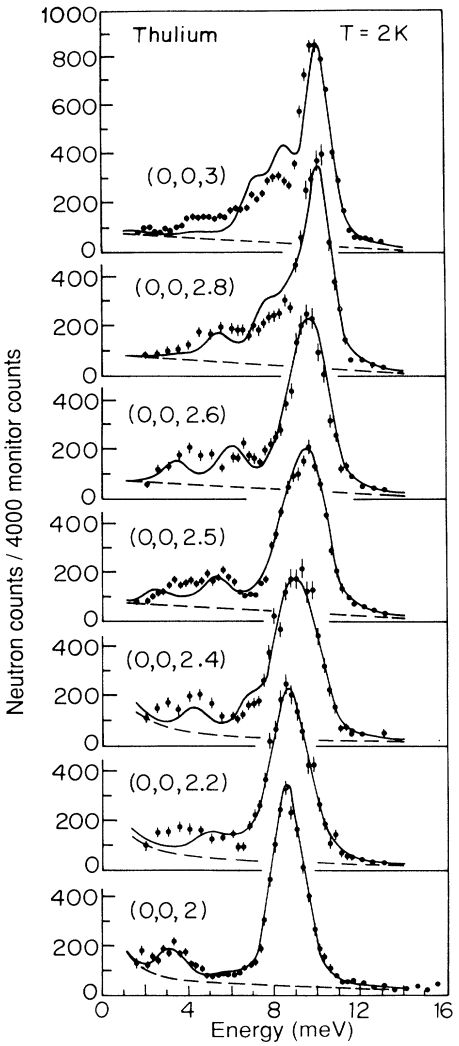

FIG. 6. Inelastic scattering spectra for Tm at 2 K, for various wave vectors along the c axis.

tors or the fitting of the magnetization curves. This deviation between experiments and the results predicted by the present model is the only one we have found which might support our earlier proposal that $\mathcal{J}(\mathbf{q})$ is somewhat temperature dependent, as suggested by the low value of the critical field in the c direction. This additional indication is not sufficiently convincing to motivate an extension of the model. Furthermore, we have made scans at 10 K, where the calculated response is nearly identical to that at 2 K; here the discrepancy was less pronounced than in Fig. 5, so it may to some extent be due to experimental uncertainties.

Because of their low intensities, the peaks due to the transverse phonons at 2 K are more sensitive to background effects and experimental uncertainties than are the spin-wave peaks. The present model, describing this scattering in terms of the simplest possible coupling between the phonons and the magnetic excitations, Eq. (12), explains the main part of the low-energy scattering. We have considered various extensions of the model without obtaining any better fit to the data. It is clear that couplings which have the same selection rules as the ϵ coupling can never explain, for instance, the excess scattering seen between the two peaks at 3 and 6 meV in the (0,0,2.6) scan, as there is an energy gap in the phonon spectrum at $q^*=0.029$ in the magnetic Brillouin zone shown in Fig. 4. The only possible way in which this scattering may be produced by a coupling to the phonons is to invoke an acoustic-optical coupling with the selection rules obtained by replacing q^* with $1/7-q^*$ (see Fig. 4). Apart from the fundamental problem of justifying such a coupling, which is only possible if the conduction electrons have a component of their polarization vector in the basal plane, the experimental indications for this coupling are not convincing. Although such a coupling would improve the fit to the (0,0,2.6) scan, in most other cases the comparison with the experimental data actually becomes worse. We conclude therefore that the differences between the calculated and experimental responses at the lower energies, at 2 K, are mainly due to experimental "noise." One possibility is that since the excess scattering is centered around 4 meV, it is a weak reminiscence of the strong peak observed at this energy in the lower quality Tm crystal studied previously by us.[1] Despite the slight reservation, we consider the determination of the ϵ coupling is trustworthy. Our model reproduces the strong effect of the coupling on the line shape of the spin-wave peaks at 2 K, which is most pronounced in the middle of the zone. These line-shape effects decrease at higher temperatures, and they are no longer important around 40 K. If the ϵ coupling was neglected, these effects would have to be explained by the exchange coupling, requiring a strong modification of $\mathcal{J}(\mathbf{q})$ at low temperatures. The good agreement obtained between the calculated and experimental phonon energies shown in Fig. 4 further supports our theory.

We do not expect that the intensity scale factor should depend on temperature. The variation due to the Debye-Waller factor can be neglected (T is small compared to the Debye temperature ~ 190 K). Therefore the intensity factors determined separately for each q value at 2 K have not been allowed to vary with temperature. The only fitting parameters at higher temperatures are the Gaussian peak widths, expected to increase because of intrinsic linewidth effects, and the background level. When the temperature is changed from 2 K to 19.8 K, only the intensity of the low-energy phononlike modes increases, since they become thermally populated. The quite oblique background used at 19.8 K in Fig. 5 is justified by supplementary data at 10 K. The latter results are not presented here because the only difference between the 10-K results and the corresponding ones at 2 K is the change of the background.

At 29.7 K the spin-wave peaks start to become slightly broader but their positions are almost unchanged. At low energies the intensities have increased by considerably more than may be accounted for by the coupling to the phonons alone. This effect has become very pronounced at the higher temperature of 39.8 K. In order to

explain the reason for this enhanced scattering, we refer to the field dependence of the crystal-field levels shown in Fig. 3. At 2 K the molecular field acting on the different moments in the four up–three down structure is calculated to vary between 0.45 and 1.77 meV. These limits are indicated in Fig. 3 by the vertical solid lines from the ground state to the lowest dipolar-coupled excited state, at 39.8 K the limits are reduced to 0.28 and 1.32 meV. At elevated temperatures the lowest excited MF levels (of predominantly $|\pm 3\rangle$ and $|\pm 4\rangle$ character) start to be thermally populated, particularly on the sites where the molecular field is small. This opens up the possibility of having dipole ($J^{\pm}$) transitions between excited states contributing to the MF Green's functions: some of these have energies around 1–2 meV. Hence the RPA model explains the strong increase in the low-energy scattering which starts to appear at 29.7 K, well below T_N, as being due to transitions between excited crystal-field levels. This feature has allowed us to make a rather accurate determination of the crystal-field parameters, since a small change of B_4^0, from zero to the value derived in the dilute systems, increases the low-energy intensity by nearly a factor of 2 at 39.8 K.

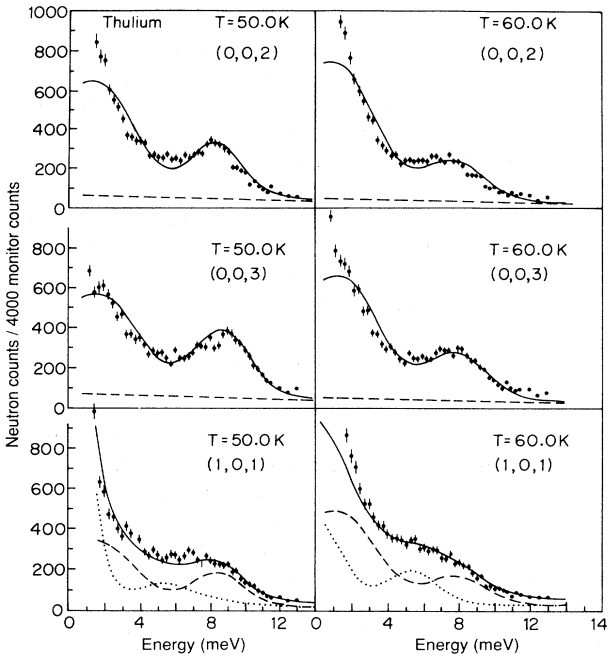

FIG. 7. The magnetic scattering function for Tm below and above T_N. Results for two wave vectors along the c axis, and at (1,0,1) are shown. The scattering function at (1,0,1) is a sum of the basal-plane and the cc components. The calculated contributions of the two different components are indicated by the signatures (– –) and (· · ·), respectively.

B. Results near T_N

Figure 7 presents the results at 50 and 60 K, i.e., just below and above $T_N = 57.5$ K. When the scattering vector is parallel to the c axis, the trends seen at lower temperatures can still be followed. The most remarkable feature is that, except for some increase in the linewidth, very little changes when the ordered moment disappears. The phonon coupling is found to be unimportant at these temperatures. Above T_N, where only diagonal couplings are allowed, it simply vanishes at the two vectors considered [$\mathcal{J}_{44}(\mathbf{q},\omega)=0$ for $q^*=0$ or 1]. The only effect which is not accounted for by the RPA theory is the excess scattering in the zero-energy limit. We consider this to be a nonlinear effect deriving from the critical fluctuations occuring near T_N. Although the extra elastic scattering disturbs the comparison at low energies, we note that the calculated peak at about 2 meV is clearly visible in the experimental results as a shoulder on the elastic peak, most pronounced at (0,0,3). The inelastic excitation seen around 8 meV in the paramagnetic phase might, at first, be regarded as a nonlinear spin wave appearing because of strong critical fluctuations. However, the RPA theory accounts accurately for both the position and the scattering intensity of this excitation, predicting it to be predominantly a crystal-field transition from the nearly doubly degenerate $|\pm 6\rangle$ ground state to the excited doublet ($0.94|\pm 5\rangle - 0.33|\pm 1\rangle$). The dispersion of this mode is very weak at 60 K. The calculations indicate that the energies lie between 7.8 and 8.0 meV at 60 K, which should be compared with corresponding values of 8.4 and 9.2 meV below T_N at 50 K, consistent with the experiments.

The critical fluctuations should be more important for the cc component of the susceptibility, as this is the component which diverges at the critical point. This component cannot be measured separately with neutrons, but it contributes to the scattering in scans with $\kappa=(1,0,1+q^*)$. In this case the structure factor of the hcp lattice implies

$$S(\kappa,\omega) \propto \mathrm{Im}[3G_0^{\alpha\beta}(q_c^*=q^*,\omega)+G_0^{\alpha\beta}(q_c^*=1-q^*,\omega)]$$

i.e., the correlation function is a linear combination of the acoustic and optical responses. Furthermore, the polarization factor means that the basal-plane component and the cc component add in $S(\kappa,\omega)$, with their relative weights being, respectively, 0.62 and 0.38 at (1,0,1). The results measured for this scattering vector at 50 and 60 K are shown in Fig. 7. The calculated longitudinal response includes a strong elastic peak, most pronounced at 50 K, and in order to fit the tail of this peak we have allowed the linewidth to be slightly more narrow for the cc component than for the basal-plane component. This is a realistic possibility as the two components are independent of each other within RPA.

The quantitative fit obtained for the c-axis scans, together with the equally good description of the (1,0,1) scattering clearly indicates that the cc component must indeed contain an inelastic peak at the position and of magnitude calculated. There are two crystal-field (J_z) transitions, both with an energy difference slightly larger than 5 meV, which explain the appearance of the inelastic peak in the longitudinal response function, and they are

shown by the vertical dashed lines in Fig. 3. We have made other $(1,0,1+q^*)$ scans at different q^* values, with results in accord with this interpretation. Except for the diverging behavior of the elastic peak, the dispersive effects were found to be very small. The RPA model even gave a correct description of the inelastic scattering, for $\hbar\omega > 2$ meV, at the critical point, $T = T_N$ and $q^* = -0.27$. At 39.8 K only the elastic peak in the *cc* component remains of any importance, and this peak rapidly disappears at decreasing temperatures, consistent with our experimental observations.

C. Linewidth effects

Finally we discuss briefly the broadening effects detected in the scattering functions. As already specified, the calculations were performed assuming a Lorentzian line shape for the excitations characterized by a width $2\hbar\epsilon = 0.6$ meV. The results thus obtained were then convoluted with a Gaussian of width w $(=2.35\sigma)$ varied so as to obtain agreement with the data. The combined total width (FWHM), $\Delta_{1/2}$, obtained from the values of $\hbar\epsilon$ and w at (0,0,2), (0,0,2.5), and (0,0,3) is shown in Fig. 8 as a function of temperature. At 2 K w varies between about 0.9 and 1.1 meV, and the result in Fig. 8 is derived from the average, as is also the case at the higher temperatures. The value $\Delta_{1/2} \simeq 1.35$ meV at zero temperature is close to the width of the instrumental resolution function (1.2 meV). The instrumental resolution function should be independent of temperature and the steady increase of $\Delta_{1/2}$ with temperature must be ascribed to intrinsic linewidth effects. Due to the large spin-wave energy gap and the relative weakness of the RKKY-exchange interaction, these effects should be very small in the low-temperature limit. In Tb the linewidth of the spin waves arising from scattering against electron-hole pair excitations of the conduction electrons is about 0.4 meV at zero temperature (see Ref. 8 and references therein). This effect scales with $(g-1)^2$, and considering that the other spin-wave parameters determining the width are nearly the same in the two metals, the RKKY contribution to $\Delta_{1/2}$ in Tm should be only about 0.05 meV. Assuming that $\Delta_{1/2}$ at zero temperature is determined by the instrumental resolution function alone, we may deduce the intrinsic width, also shown in Fig. 8. Most interestingly, this intrinsic width is very well described by the exponential function $\exp(-E_0/T)$ with the activation energy, $E_0 = 85$ K $(=7.3$ meV), close to the crystal-field splitting between the ground state and the dipolar-coupled excited state. This is exactly the behavior expected, to leading order, in a crystal-field system, see for example the discussion[16] of the linewidth effects in Pr.

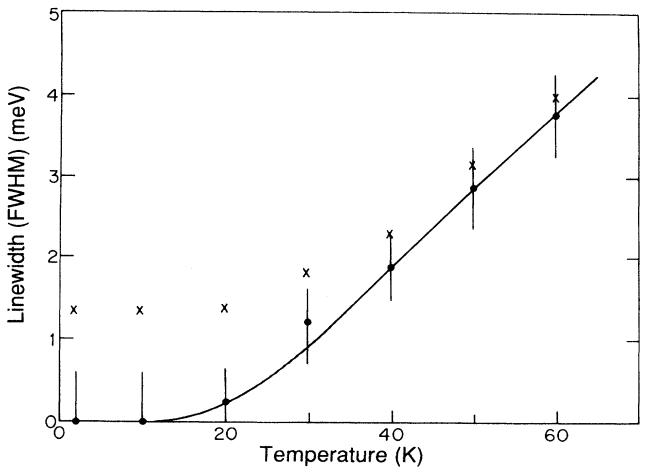

FIG. 8. The total width at half maximum intensity, $\Delta_{1/2}$, as a function of temperature. The crosses denote the values derived including the instrumental resolution. The circles indicate the estimated results for the intrinsic linewidth, assuming the total width in the zero temperature limit to be determined by the instrumental resolution alone. The line is a fit to the intrinsic width proportional to $\exp(-E_0/T)$ with $E_0 = 85$ K.

VI. CONCLUSIONS

The magnetic scattering function in the *c* direction of thulium has been investigated in considerable detail, both in the antiferromagnetic four-up–three-down phase and in the paramagnetic phase just above T_N. The RPA theory developed in Sec. II adequately describes most of the different phenomena observed, and it therefore provides a reliable basis for determining the fundamental magnetic interactions in Tm. Although Tm belongs to the heavy part of the series of rare-earth metals, the scaling factor $(g-1)^2$ for the RKKY-exchange interaction is small, and the Néel temperature in Tm is low compared to the crystal-field energy-splittings. The crystal-field effects are therefore more important in this metal than in the other heavy rare-earths. Thus, besides the spin-wave excitations at low temperatures, well-defined crystal-field excitations have been detected above and below T_N, both in the basal-plane component and, indirectly, in the *cc* component of the scattering function.

The low-temperature results revealed the presence of a rather strong coupling between the spin waves and the transverse phonons. From the analysis we conclude that most of the magnetic scattering produced by these phonons can be explained by a nearest-neighbor magnetoelastic ϵ coupling. Although some minor discrepancies remain, there is no convincing evidence for any additional, more complicated, coupling between the spin waves and the phonons. The derived coupling parameter predicts a reduction of about 20% of the elastic constant c_{44} from its nonmagnetic value, in the zero temperature limit. Another measure of the strength of this coupling is that its effects, at low temperatures, on the dispersion of the spin waves are nearly as large as those produced by $\mathcal{J}(\mathbf{q})$. These effects decrease when the temperature is increased, and they are almost negligible close to T_N.

The parameter B_2^0 was determined from the anisotropy between the high-temperature susceptibilities. The remaining crystal-field parameters were derived from the excitation spectrum, i.e., from the spin-wave energy gap at zero temperature and from the low-lying transitions between the excited crystal-field states at elevated tem-

peratures. Although these effects are quite sensitive to any change of the parameters, we can only claim that the lower part of the crystal-field level scheme has been accurately established, as the extra condition used $B_6^6 = -(77/8)B_6^0$ may not be exact. Nevertheless, it is interesting to note that the crystal-field parameters derived for Tm, with its relatively weak two-ion coupling, are close to those determined earlier[12] for the dilute systems. This situation is comparable with that found in Pr (see Ref. 16 and references therein), where the RKKY interaction is also rather small.

The RKKY-exchange coupling in the c direction of Tm was determined by the magnetization data and the temperature dependence of the magnetic structure, almost without need to refer to the excitation energies. This procedure led to one unresolved discrepancy, namely, that the critical field required for aligning the moments ferromagnetically along the c axis was calculated to be about 50% larger than is observed at low temperature. This effect may be due to an abrupt change of $\mathcal{J}(\mathbf{0})$ at the critical field, or it may indicate that $\mathcal{J}(\mathbf{q})$ is somewhat temperature dependent. In the absence of clear evidence, the possible temperature dependence of $\mathcal{J}(\mathbf{q})$ was ignored in the analysis. The two-ion coupling determining the magnetization is actually $\mathcal{J}^{cc}(\mathbf{q})$ whereas the spin-wave energies are only affected by $\mathcal{J}^{bb}(\mathbf{q})$. This means that the minor discrepancy found in the line shape of the spin-wave scattering at (0,0,3) may, alternatively, be explained by an anisotropic two-ion coupling. In the analysis we assumed that the only difference between the two components arises from the magnetic dipole interaction, and the good description of the experimental results allows us to conclude that any other anisotropic two-ion effects are small in Tm. The reason for this difference between Tm and the other heavy rare-earth metals, in most of which anisotropic two-ion couplings are important,[7,8] may simply be that other two-ion interactions scale in the same way as the RKKY coupling. Also the higher symmetry in Tm, where there is no component of the ordered moments in the basal plane as in the other heavy rare-earths, may play a role.

The RKKY coupling, divided by the scale factor $(g-1)^2$, is compared in Fig. 9 for the six magnetic heavy rare-earth metals.[7,17–21] The most pronounced feature in this comparison is that the strong peak in $\mathcal{J}(\mathbf{q})$ in Tm develops gradually in a systematic way through the series from Gd, Tb, Dy, Ho, Er to Tm. Another interesting point is that $[\mathcal{J}(\mathbf{q})-\mathcal{J}(\mathbf{0})]/(g-1)^2$ remains fairly constant at the Brillouin-zone boundary.

The RPA theory accounts very well for most of our experimental observations. One significant shortcoming is that the theory does not describe the transverse quasielastic scattering occuring close to T_N, not surprisingly since this is a critical phenomenon. The only other deficiency of the theory is that linewidth effects are not included *a priori;* however, they have been isolated in the analysis of the experimental results. These effects are not very dependent on the wave vector, but they increase exponentially with temperature in the way expected for a crystal-field system.

The behavior of the spin-wave spectrum in Tm, in directions other than the direction considered here, is expected to be very similar. We have made some preliminary experiments at 2 K, with $\mathbf{q}$ lying in the basal plane, and, as anticipated, the dispersive effects are found to be small. Our determination of $\mathcal{J}(\mathbf{q})$ in the c direction relied much on the assumption that the magnetization measurements provide a good first approximation. In other directions of $\mathbf{q}$ the exchange coupling will have to be determined from the excitation energies alone, and it will be very hard to do that for the antiferromagnetic phase of Tm. One other possibility is to study the ferromagnetic phase induced when applying a field larger than the critical field in the c direction. In this case there will be no more than two spin-wave branches at each $\mathbf{q}$, and it should be possible to resolve them, leading to a more direct determination of $\mathcal{J}(\mathbf{q})$. It would also be interesting to repeat the measurements along the c axis in the ferromagnetic phase, in order to see whether any changes of $\mathcal{J}(\mathbf{q})$ occur.

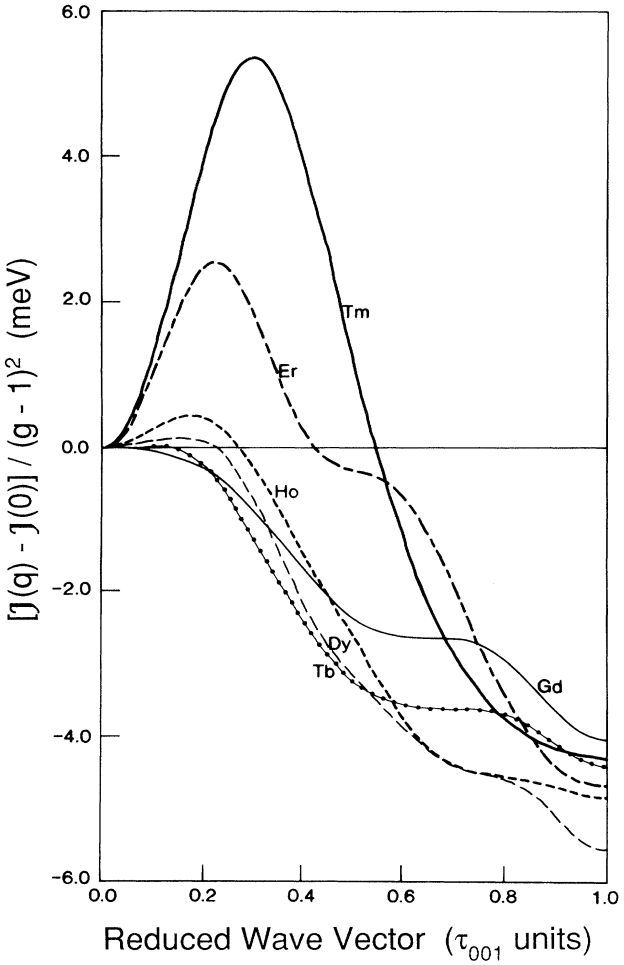

FIG. 9. The exchange coupling $[\mathcal{J}(\mathbf{q})-\mathcal{J}(\mathbf{0})]/(g-1)^2$ in all the magnetic heavy rare-earth metals. The experimental results are from Refs. 17, 18, 19, and 7 in the respective cases of Gd, Tb, Dy, and Ho, and from Refs. 20 and 21 in the case of Er.

ACKNOWLEDGMENTS

We would like to thank J. L. Martinez for his help during our experiment at the Institut Laue Langevin. We thank also J. A. Fernandez-Baca, R. M. Nicklow, and J. J. Rhyne for providing us with the results of their measurements before publication. Useful discussions with them and with J. F. Cooke and A. R. Mackintosh are gratefully acknowledged. One of us (J.J.) wishes to acknowledge the hospitality of the Rutherford Appleton Laboratory during a visit. This research was financially supported by the Science and Engineering Research Council.

[1]K. A. McEwen and U. Steigenberger, J. Phys. (Paris) **49**, C8, 335 (1988).
[2]J. A. Fernandez-Baca, R. M. Nicklow, and J. J. Rhyne, J. Appl. Phys. **67**, 5283 (1990).
[3]W. C. Koehler, J. W. Cable, E. O. Wollan, and M. K. Wilkinson, Phys. Rev. **126**, 1672 (1962).
[4]T. O. Brun, S. K. Sinha, N. Wakabayashi, G. H. Lander, L. R. Edwards, and F. H. Spedding, Phys. Rev. B **1**, 1251 (1970).
[5]D. B. Richards and S. Legvold, Phys. Rev. **186**, 508 (1969).
[6]P. B. Fynbo, J. Phys. F **7**, 2179 (1977).
[7]C. C. Larsen, J. Jensen, and A. R. Mackintosh, Phys. Rev. Lett. **59**, 712 (1987).
[8]J. Jensen, J. Magn. Magn. Mat. **29**, 47 (1982).
[9]J. Jensen, J. Phys. (Paris) **49**, C8, 351 (1988).
[10]J. G. Houmann and R. M. Nicklow, Phys. Rev. B **1**, 3943 (1970).
[11]J. Jensen and J. G. Houmann, Phys. Rev. B **12**, 320 (1975).
[12]P. Touborg, Phys. Rev. B **16**, 1201 (1977).
[13]S. B. Palmer, E. W. Lee, and M. N. Islam, Proc. R. Soc. London A **338**, 341 (1974).
[14]R. Ramji Rao and A. Rajput, Z. Naturforsch. A **34**, 200 (1979).
[15]T. O. Brun and G. H. Lander, Phys. Rev. Lett. **23**, 1295 (1969).
[16]J. Jensen, K. A. McEwen, and W. G. Stirling, Phys. Rev. B **35**, 3327 (1987).
[17]W. C. Koehler, H. R. Child, R. M. Nicklow, H. G. Smith, R. M. Moon, and J. W. Cable, Phys. Rev. Lett. **24**, 16 (1970).
[18]J. Jensen, J. G. Houmann, and H. Bjerrum Møller, Phys. Rev. B **12**, 303 (1975).
[19]R. M. Nicklow, N. Wakabayashi, M. K. Wilkinson, and R. E. Reed, Phys. Rev. Lett. **26**, 140 (1971).
[20]R. M. Nicklow, N. Wakabayashi, M. K. Wilkinson, and R. E. Reed, Phys. Rev. Lett. **27**, 334 (1971).
[21]J. Jensen, J. Phys. F **4**, 1065 (1974).